

Atomic frustrated impurity states in Weyl metals

W. N. Mizobata,¹ Y. Marques,² M. Penha,¹ J. E. Sanches,¹ L. S. Ricco,¹ M. de Souza,³ I. A. Shelykh,^{2,4} and A. C. Seridonio^{1,3,*}

¹*São Paulo State University (Unesp), School of Engineering, Department of Physics and Chemistry, 15385-000, Ilha Solteira-SP, Brazil*
²*Department of Physics, ITMO University, St. Petersburg 197101, Russia*

³*São Paulo State University (Unesp), IGCE, Department of Physics, 13506-970, Rio Claro-SP, Brazil*

⁴*Science Institute, University of Iceland, Dunhagi-3, IS-107, Reykjavik, Iceland*

We theoretically analyze the effect of the inversion symmetry breaking on the structure of the impurity molecular states in Weyl metals. We show that for the case of a highly noncentrosymmetric Weyl metallic host, the standard picture of the alternating bonding and antibonding orbitals breaks down, and a qualitatively different frustrated atomic state emerges. This is a consequence of the pseudogap closing and related delicate Fano interplay between intra- and inter-impurity scattering channels.

I. INTRODUCTION

Dirac-Weyl equation [1], which first appears in the context of the relativistic quantum field theory, where it describes massless fermions, such as neutrinos, recently found its application in the domain of condensed matter physics. The existence of Dirac-Weyl fermions, quasi-relativistic quasiparticles, was unambiguously demonstrated for the family of the gapless binary alloys, such as Na₃Bi, Cd₃As₂, TaAs, NbAs and TaP [2–12]. The pair of the Dirac cones, present in these materials, can be split into two Weyl nodes with opposite chirality, if certain symmetry (inversion or time-reversal) is broken [13]. As a result, a topological Weyl material with unusual characteristics, such as Fermi arcs, chiral anomaly and exotic Hall effects [13–19], emerges. The peculiar band structure of Weyl systems has dramatic impact on the electronic structure of impurities [20–27]. In particular, as it was recently shown by some of us, chiral magnetic chemical bounds for a pair of impurities can appear in Weyl semimetals with energy degenerate Weyl nodes shifted in \mathbf{k} space with respect to each other [27].

In this communication, we consider the structure of impurity molecular states in Weyl metals, where two Weyl nodes are located at the same \mathbf{k} , but are shifted in energy. We demonstrate that in the geometry corresponding to two Anderson-like impurities [28] shown in Fig. 1, bonding and antibonding molecular states evolve into an atomic frustrated state marked by two Hubbard bands [29], with increase of the energy splitting between the two Weyl nodes. In this regime, the closing of the host pseudogap occurs, which leads to the dominance of the destructive Fano interference [30, 31] in the intra-impurity scattering channel, which is opposite to what happens in the corresponding inter-impurity channel revealing resonant behavior. The reported crossover can be realized by application of external stress [13] and experimentally detected with use of the STM techniques.

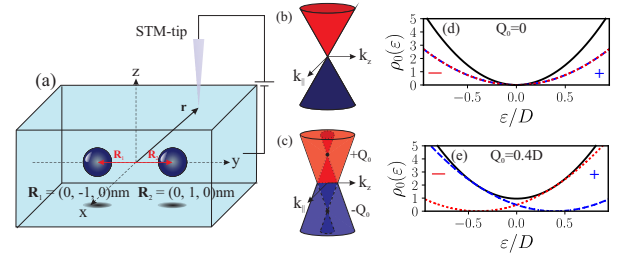


Figure 1. (Color online) Panel (a): Sketch of the considered system, consisting of a pair of impurities placed inside a Weyl metal close to its interface. The positions of the impurities are characterized by the vectors $\mathbf{R}_{1,2}$. The impurity molecular states can be probed on the surface of the host by an STM tip, whose location is characterized by the vector \mathbf{r} . Panel (b): Sketch of the dispersion, characteristic for a Dirac semimetal with two degenerated Dirac cones. The pseudogap is formed around the Dirac point, where the host Density of States (DOS) $\rho(\varepsilon) = 0$. Panel (c): Sketch of the dispersion, characteristic for the Weyl metal. The degeneracy of the Dirac cones is lifted due to the breaking of the inversion symmetry, and a pair of Weyl nodes vertically shifted with respect to each other appears. The pseudogap is closed due to the lifting of the degeneracy of the Weyl nodes. Panel (d): DOS $\rho(\varepsilon)$ of a Dirac semimetal. Panel (e): DOS $\rho(\varepsilon)$ of a Weyl metal. The plus and minus signs identify the DOS resolved in opposite chiralities.

II. THE MODEL

The Hamiltonian of the system sketched in Fig. 1 can be represented as:

$$\mathcal{H} = \sum_{\mathbf{k}} \psi^\dagger(\mathbf{k}) (H_+ \oplus H_-) \psi(\mathbf{k}) + \varepsilon_d \sum_{j\sigma} d_{j\sigma}^\dagger d_{j\sigma} + U \sum_j d_{j\uparrow}^\dagger d_{j\uparrow} d_{j\downarrow}^\dagger d_{j\downarrow} + \sum_{j\mathbf{k}} \tilde{d}_j^\dagger \tilde{V}_{j\mathbf{k}} \psi(\mathbf{k}) + \text{H.c.}, \quad (1)$$

where $H_\chi(\mathbf{k}) = \chi(v_F \boldsymbol{\sigma} \cdot \mathbf{k} + \sigma_0 Q_0)$ is the Dirac-Weyl Hamiltonian of the host, corresponding to the two Dirac cones shifted vertically in energy (see Fig. 1(c)), $\boldsymbol{\sigma}$ stands

* corresponding author: antonio.seridonio@unesp.br

for the vector of Pauli matrices, σ_0 is the unity matrix, $\chi = \pm 1$ corresponds to the Weyl nodes chirality, Q_0 is the characteristic parameter defining the energy splitting between the Weyl nodes ($Q_0 \neq 0$ corresponds to a Weyl metal, $Q_0 = 0$ to a Dirac semimetal), v_F is the Fermi velocity, $\psi(\mathbf{k}) = (c_{\mathbf{k}+\uparrow}, c_{\mathbf{k}+\downarrow}, c_{\mathbf{k}-\uparrow}, c_{\mathbf{k}-\downarrow})^T$ is the four-spinor operator describing the electronic states in the host $c_{\mathbf{k}\chi\sigma}^\dagger, c_{\mathbf{k}\chi\sigma}$ with wave vector \mathbf{k} , chirality χ and spin σ . The operators $d_{j\sigma}^\dagger, d_{j\sigma}$ describe the electronic states of individual impurities ($j = 1, 2$) with single-particle energies ε_d and on-site Coulomb correlation energy U . The term, containing the two-spinor $\tilde{d}_j^\dagger = (d_{j\uparrow}^\dagger, d_{j\downarrow}^\dagger)$, couples the impurities to the host, via the matrix

$$\tilde{V}_{j\mathbf{k}} = v_0 \begin{pmatrix} e^{i\mathbf{k}\cdot\mathbf{R}_j} & 0 & e^{i\mathbf{k}\cdot\mathbf{R}_j} & 0 \\ 0 & e^{i\mathbf{k}\cdot\mathbf{R}_j} & 0 & e^{i\mathbf{k}\cdot\mathbf{R}_j} \end{pmatrix}, \quad (2)$$

with v_0 being the coupling strength.

The electronic characteristics of the system are determined by its Local Density of States (LDOS) $\rho(\varepsilon, \mathbf{r})$, which can be found from the Green's functions (GF) of the host in the energy domain, $\tilde{\mathcal{G}}_{\chi\chi'\sigma}(\varepsilon, \mathbf{r})$ [32] defined as the time-Fourier transform of $\mathcal{G}_{\chi\chi'\sigma}(t, \mathbf{r}) = -i\theta(t) \langle \{\psi_{\chi\sigma}(t, \mathbf{r}), \psi_{\chi'\sigma}^\dagger(0, \mathbf{r})\} \rangle_{\mathcal{H}}$, with $\psi_{\chi\sigma}(t, \mathbf{r}) = \sum_{\mathbf{k}} e^{i\mathbf{k}\cdot\mathbf{r}} c_{\mathbf{k}\chi\sigma}(t)$ being the field operator of the host conduction states with spin σ and chirality χ . The LDOS reads [26, 27, 32]:

$$\rho(\varepsilon, \mathbf{r}) = -\frac{1}{\pi} \sum_{\chi\chi'} \text{Im} \{ \tilde{\mathcal{G}}_{\chi\chi'\sigma}(\varepsilon, \mathbf{r}) \} = \rho_0 + \sum_{jj'} \delta\rho_{jj'}, \quad (3)$$

where the first term in this expression describes the host DOS $\rho_0 = \sum_{\chi} \frac{3\varepsilon^2}{D^3}$, with D as the energy cutoff and $\varepsilon_{\chi} = \varepsilon - \chi Q_0$, and the second term is the correction to the LDOS induced by the host-impurity coupling:

$$\delta\rho_{jj'}(\varepsilon, \mathbf{r}) = -\frac{1}{\pi v_0^2} \sum_{\chi\chi'} \text{Im} [\Sigma_{\chi\sigma}^+(\mathbf{r} - \mathbf{R}_j) \tilde{\mathcal{G}}_{j\sigma|j'\sigma}(\varepsilon) \times \Sigma_{\chi'\sigma}^-(\mathbf{r} - \mathbf{R}_{j'})], \quad (4)$$

where \mathbf{R}_j describes the coordinates of the two impurities. The terms with $j' = j$ and $j' \neq j$ correspond to intra- and inter-impurity scattering channels, respectively, and

$$\Sigma_{\chi\sigma}^{\pm}(\mathbf{r}) = -\frac{3\pi v_F v_0^2}{2D^3} \frac{e^{-i|\mathbf{r}| \frac{\varepsilon_{\chi}}{v_F}}}{|\mathbf{r}|} \left[\varepsilon_{\chi} \pm \chi\sigma \left(\varepsilon_{\chi} + i \frac{v_F}{|\mathbf{r}|} \right) \right] \quad (5)$$

are self-energy terms responsible for the spatial modulation of the LDOS. Following Ref.[25], to obtain Eq.(5), we have evaluated the noninteracting part of the GF $v_0^2 \tilde{\mathcal{G}}_{\chi\chi'\sigma}(\varepsilon, \mathbf{r})$ (the corresponding one which solely considers the first term in Eq.(1)), by means of an expansion of the plane wave $e^{i\mathbf{k}\cdot\mathbf{r}}$ within $\tilde{\psi}_{\chi\sigma}(\varepsilon, \mathbf{r})$ (the Fourier transform of $\psi_{\chi\sigma}(t, \mathbf{r})$) into spherical harmonics terms, according to the Rayleigh equation, particularly for $D \gg \varepsilon$ [23, 25].

$\tilde{\mathcal{G}}_{j\sigma|j'\sigma}(\varepsilon)$ is the time-Fourier transform of the impurities GFs, $\mathcal{G}_{j\sigma|j'\sigma}(t) = -i\theta(t) \langle \{d_{j\sigma}(t), d_{j'\sigma}^\dagger(0)\} \rangle_{\mathcal{H}}$. Away from the Kondo regime [33], Hubbard-I approximation [26, 27, 29, 32] can be applied, which gives:

$$\tilde{\mathcal{G}}_{j\sigma|j'\sigma}(\varepsilon) = \frac{\lambda_j^{\bar{\sigma}}}{g_{j\sigma|j\sigma}^{-1}(\varepsilon) - \lambda_j^{\bar{\sigma}} \Sigma_{\sigma}^+(\mathbf{R}_{12}) g_{j'\sigma|j'\sigma}(\varepsilon) \lambda_{j'}^{\bar{\sigma}} \Sigma_{\sigma}^-(\mathbf{R}_{12})}. \quad (6)$$

Here $\bar{\sigma} = -\sigma$, $j' \neq j$, $\mathbf{R}_{12} = \mathbf{R}_1 - \mathbf{R}_2$, $\Sigma_{\sigma}^{\pm}(\mathbf{r}) = \sum_{\chi} \Sigma_{\chi\sigma}^{\pm}(\mathbf{r})$,

$$g_{j\sigma|j\sigma}(\varepsilon) = \frac{1}{\varepsilon - \varepsilon_{j\sigma} - \Sigma_0} \quad (7)$$

is the single-impurity noninteracting GF,

$$\Sigma_0 = \frac{3v_0^2}{2D^3} \sum_{\chi} \varepsilon_{\chi}^2 \left(\ln \left| \frac{D + \varepsilon_{\chi}}{D - \varepsilon_{\chi}} \right| - \frac{2D}{\varepsilon_{\chi}} - i \right) \quad (8)$$

as the local self-energy,

$$\lambda_j^{\sigma} = 1 + \frac{U}{g_{j\bar{\sigma}|j\bar{\sigma}}(\varepsilon) - U} \langle n_{j\sigma} \rangle \quad (9)$$

is the spectral weight and

$$\langle n_{j\sigma} \rangle = -\frac{1}{\pi} \int_{-\infty}^{+\infty} n_F(\varepsilon) \text{Im} [\tilde{\mathcal{G}}_{j\sigma|j\sigma}(\varepsilon)] d\varepsilon \quad (10)$$

is the impurity occupation [34]. The crossed GF reads

$$\tilde{\mathcal{G}}_{j\sigma|j'\sigma}(\varepsilon) = g_{j\sigma|j\sigma}(\varepsilon) \lambda_j^{\bar{\sigma}} \Sigma_{\sigma}^{\pm}(\mathbf{R}_{jj'}) \tilde{\mathcal{G}}_{j'\sigma|j'\sigma}(\varepsilon), \quad (11)$$

in which the \pm signs correspond to $j = 1, j' = 2$ and $j = 2, j' = 1$, respectively. We emphasize that to close the set of Eqs. (6), (9) and (11) we have followed, as mentioned previously, the Hubbard-I scheme [26, 27, 29, 32]. It truncates the GFs of the Hamiltonian (Eq.(1)) by taking into account the Coulomb blockade regime [29, 32] and neglecting the Kondo correlations, where spin-flip processes dominate [33]. Thus, in applying the equation of motion procedure (EOM) to evaluate such GFs [32], those showing spin-flip scattering should be disregarded. By this manner, the impurity occupation $\langle n_{j\sigma} \rangle$ (Eq.(10)) is then determined off the Kondo limit [34], by performing a self-consistent calculation. The unique regime in which the equations above are exact is for $U = 0$.

In the case of uncorrelated impurities, realized when $|\mathbf{R}_{12}| \gg v_F v_0^2 / D^3$, $\Sigma_{\sigma}^{\pm}(\mathbf{R}_{jj'}) = 0$ and $\delta\rho_{jj'} = 0$, Eq. (6) has two poles (the so-called Hubbard resonant bands [29]), appearing in $\delta\rho_{jj'}$. The host-mediated inter-impurity correlations lead to the splitting of these poles, which corresponds to the formation of the impurity molecular bands even in the absence of the direct hopping term between the impurities [26].

III. RESULTS AND DISCUSSION

In our following consideration, we use model parameters: $|\mathbf{R}_{12}| = 2$ nm, $\varepsilon_d = -0.07D$, $v_0 = -0.14D$, $U = 0.14D$, $v_F \approx 3$ eVÅ and $D \approx 0.2$ eV [26, 27]. We suggest that the impurities are buried at the distance of 1 nm below the top surface of the Dirac-Weyl material, and are placed in the points $\mathbf{R}_1 = (0, -1, 0)$ nm and $\mathbf{R}_2 = (0, 1, 0)$ nm (see Fig. 1).

Fig. 2 illustrates the evolution of the spatial profiles of the LDOS at the surface of the host, given by Eq. (3), which can be probed by an STM tip, with increase of the parameter Q_0 , describing the breaking of the inversion symmetry. In panel (a) the case of a Dirac semimetal with degenerated Weyl nodes, corresponding to $Q_0 = 0$, is illustrated. Molecular orbitals of the bonding and antibonding type are formed, and the profile corresponding to the latter one, with maxima of the LDOS centered at the points where the impurities are located, is shown. We stress that due to the peculiarities of the band structure of the Dirac host, the antibonding state has lower energy as compared to the bonding state, as it was demonstrated in Ref. [26]. The increase of the parameter Q_0 leads to the broadening of the LDOS peaks. Still, if values of Q_0 are moderate, the LDOS profiles remain qualitatively the same as for $Q_0 = 0$, and still can be described in terms of the formation of an antibonding molecular state, as it is illustrated in the panel (b). However, if the value of the parameter Q_0 becomes sufficiently large, the profile of the LDOS dramatically changes. It becomes depleted in the broad region around the impurities, and corresponds to a frustrated centrosymmetric configuration characteristic to a frustrated atomic state, as it is shown in the panel (c).

To shed more light on the underlying mechanisms of its formation, we have analyzed separately different contributions to the LDOS induced by the impurities, as illustrated by Figs. 3 and 5.

Fig. 3 shows the plots of $\delta\rho_{jl}(\varepsilon, \mathbf{r})$ as a function of the energy for one particular tip position $\mathbf{r} = (1, 1, 1)$ nm (the change of this latter does not affect the results qualitatively). Both contributions from intra-impurity ($j = l$) and inter-impurity ($j \neq l$) are shown. In panel (a), corresponding to the case of a Dirac host with $Q_0 = 0$, one clearly sees the presence of the four peaks in $\delta\rho_{jj}$, corresponding to well resolved Hubbard bands and describing the formation of bonding and antibonding molecular orbitals, which stem from single-impurity bands centered around $\varepsilon_d < 0$ and $\varepsilon_d + U > 0$. For the considered parameters, the lowest energy peak corresponds to the antibonding state (pointed by the red arrow) and next peak to the bonding molecular state (pointed by the green arrow) [26]. The crossed term $\delta\rho_{jl}$, with $j \neq l$ exhibits two resolved pairs of peaks and Fano dips instead. The increase of the parameter Q_0 leads to the broadening of the peaks and Fano dips (panel (b), $Q_0 = 0.1D$). At some point, the peaks corresponding to the bonding and antibonding states merge, giving rise to intermediate Fano

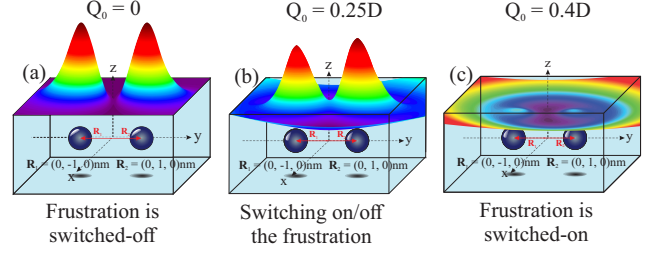


Figure 2. (Color online) Panel (a): Spatial profile of the LDOS, corresponding to the antibonding state of a pair of impurities, placed inside a Dirac semimetal ($Q_0 = 0$). Panel (b): Spatial profile of the LDOS for a pair of impurities, placed inside a Weyl metal with moderate value of $Q_0 = 0.25D$. Panel (c): Spatial profile of the LDOS, corresponding to the frustrated atomic state, for a pair of impurities, placed inside a Weyl metal with large value of $Q_0 = 0.4D$.

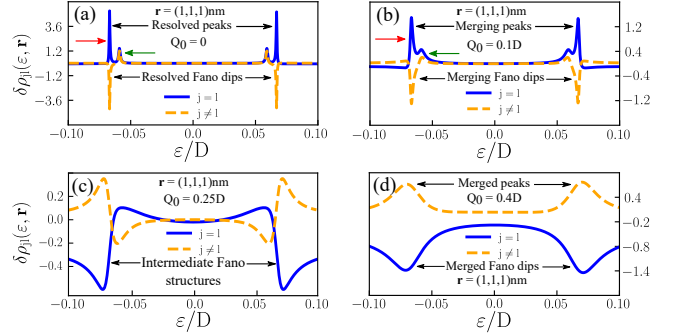


Figure 3. (Color online) Impurity-induced contributions to the density of states $\delta\rho_{jl}$ as a function of energy. Position of the STM tip is fixed at $\mathbf{r} = (1, 1, 1)$ nm. Panel (a): The case of a Dirac semimetal host, $Q_0 = 0$. One clearly sees two well resolved pairs of peaks in $\delta\rho_{jj}$, centered around ε_d and $\varepsilon_d + U$ and corresponding to bonding (indicated by green arrow) and antibonding (indicated by red arrow) molecular orbitals. Panel (b): The case of a Weyl metal host with small value of $Q_0 = 0.1D$. The peaks corresponding to the molecular states become broadened, but are still clearly resolved. Panel (c): The case of a Weyl metal host with moderate value of $Q_0 = 0.25D$. Intermediate Fano structures with merged peaks and dips appear. Panel (d): The case of a Weyl metal host with large value of $Q_0 = 0.4D$. Broad plateau in the density of states flanked by a pair of the merged peaks or dips is formed around $\varepsilon = 0$. Transition to the regime of atomic frustrated state occurs, as seen in Fig. 2(c).

lineshapes, with shallow minimum at $\varepsilon = 0$ (panel (c), $Q_0 = 0.25D$). Further increase of Q_0 leads to the formation of a broad plateau in the density of states around $\varepsilon = 0$, flanked by a pair of merged peaks for $j \neq l$, or merged dips for $j = l$ (panel (d), $Q_0 = 0.4D$). The presence of only two resolved Hubbard bands is typical for a pair of uncorrelated impurities. However, in our case the amplitudes $\delta\rho_{jl} \neq 0$ for $j \neq l$, which means that molecular binding still persists, although in the unusual

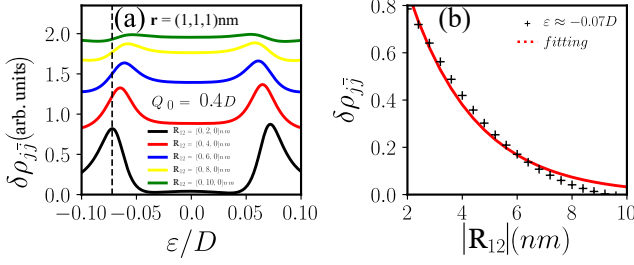


Figure 4. (Color online) Panel (a): Induced LDOS term $\delta\rho_{j\bar{j}}$ ($j = 1, \bar{j} = 2$ and $j = 2, \bar{j} = 1$) for $Q_0 = 0.4D$ with STM tip at $\mathbf{r} = (1, 1, 1)$ nm as a function of energy for several values of \mathbf{R}_{12} . For a sake of clarity, we present each case vertically shifted, thus making explicit that the increasing of $|\mathbf{R}_{12}|$ leads to the LDOS $\delta\rho_{j\bar{j}}$ vanishing. Hence, such a quenching reveals the crossover from the profile with two Hubbard bands, characteristic of the atomic frustrated state, towards that completely flat, for the uncorrelated pair of atoms situation. Panel (b): Amplitude of $\delta\rho_{j\bar{j}}$ evaluated at the black-dashed line cut $\varepsilon \approx -0.07D$ marked in panel (a) as a function of $|\mathbf{R}_{12}|$, which exhibits an exponential-like decay (crossed-points in black). Particularly, it is fitted by $\delta\rho_{j\bar{j}}(\varepsilon \approx -0.07D) = 1.96 \exp(-0.41|\mathbf{R}_{12}|)$ (red line).

form of an atomic frustrated state. In this configuration, the role of the constructive and destructive Fano interference channels between $\delta\rho_{jj}$ and $\delta\rho_{jl}$ becomes inverted with respect to those observed in Dirac hosts, as it can be clearly seen from the comparison between panels (d) and (a).

We highlight that Figs. 2 and 3 introduce the concept of the atomic frustrated state, whose origin is genuinely of molecular-type, wherein its signatures resemble simultaneously those from uncorrelated and correlated atoms. Noteworthy, in such a scenario, the collective behavior of a diatomic molecule mimics an uncorrelated pair of atoms. Its characterization consists of electronic depletions (Fano dips) in $\delta\rho_{jj}$ around the Hubbard bands at $\varepsilon_d < 0$ and $\varepsilon_d + U > 0$, exactly as in the corresponding uncorrelated situation. Additionally and counterintuitively, a finite inter-impurities correlation ($\delta\rho_{jl} \neq 0$ with $j \neq l$) emerges as in a molecule, being identified by two Hubbard peaks instead. Hence, as this pair of atoms remains correlated through the host ($\delta\rho_{jl}$ finite, although with just two Hubbard structures), but shows itself seemingly uncorrelated ($\delta\rho_{jj}$ with two Hubbard structures, instead of four as in a molecule), then the state is considered atomically frustrated.

It is worth mentioning that as we focus on the paramagnetic case of impurities ($\langle n_{j\uparrow} \rangle = \langle n_{j\downarrow} \rangle$), the Dzyaloshinskii-Moriya interaction (DMI), which is a type of spin texture within the RKKY interaction [22, 23] for Dirac-Weyl semimetals, indeed does not rule this peculiar molecular binding here reported. The key responsible mechanism for the proposed state relies on the well-known Friedel-like oscillations [35], which according to some of us [26, 27], by working cooperatively with the

intra-impurities Coulomb repulsion, is capable of establishing molecular bonds in Dirac-Weyl hosts. Thus, in the frustration regime of the Weyl metal phase, for first ever, novel Friedel-like behavior is revealed. It consists of electronic waves that travel forth and back between the left and right impurities ($\delta\rho_{jl}$), which are entirely phase shifted by π with respect to those scattered locally by the impurities ($\delta\rho_{jj}$). As a result, $\delta\rho_{jj}$ shows two structures dominantly Fano destructive at the two Hubbard bands $\varepsilon_d < 0$ and $\varepsilon_d + U > 0$ (Fig. 3(d)), which then flank a flat metallic-type plateau in the LDOS around the Fermi energy, as we will see later on.

In order to understand the long-range behavior of the frustrated atomic state encoded by $\delta\rho_{jl}$, in Fig.4(a) we analyze such a quantity for $Q_0 = 0.4D$ and STM-tip at $\mathbf{r} = (1, 1, 1)$ nm, as a function of energy upon varying \mathbf{R}_{12} . We can clearly perceive that the pair of Hubbard bands of the atomic frustrated state become broader as we increase the inter-impurities separation, in such a way that the $\delta\rho_{jl}$ approaches a profile entirely flat, which corresponds to the case of decoupled atoms. Thus by fixing the energy, for instance at $\varepsilon \approx -0.07D$ (black-dashed line cut), it is possible to estimate how quickly $\delta\rho_{jl}$ vanishes. Fig.4(b) then makes explicit that the decay obeys an exponential-like behavior (crossed-points in black), which is fitted by $\delta\rho_{j\bar{j}}(\varepsilon \approx -0.07D) = 1.96 \exp(-0.41|\mathbf{R}_{12}|)$ (red line), where $j = 1, \bar{j} = 2$ and $j = 2, \bar{j} = 1$. Notice that for $|\mathbf{R}_{12}| = 10$ nm, the molecular bond of the atomic frustrated state is practically dissociated.

Fig. 5(a) shows that the corresponding total LDOS has very broad maximum at $\varepsilon = 0$ and a pair of the broad minima around ε_d and $\varepsilon_d + U$. We clarify that the emergence of a flat LDOS (broad plateau) in the vicinity of $\varepsilon = 0$ (the Fermi energy) is characteristic of the metallic regime of the host. This is the direct outcome of the pseudogap closing in Weyl materials with large Q_0 , for which the host DOS is enhanced at the Fermi energy. In equivalent words, it leads to the enhancement of states in the Fermi surface, exactly when the inversion symmetry is highly broken, which drives the system into the metallic Weyl regime. This comes from the increasing of the Dirac cones separation obeying blue and red shifts in the energy axis (see Fig.1(c) of the system sketch). This causes the formation of two bands. However, distinctly from the spin-orbit coupling, which resolves these bands in the spin channels, in Weyl metals such a separation occurs in the chirality degrees of freedom. The latter, we call particular attention, is defined as the spin projection over the linear momentum, contrasting the spin-orbit coupling, which instead, projects the former on the angular momentum. Thus, by integrating all momentum states split in energy, leads to two branches in the background DOS $\rho_0(\varepsilon)$, which are resolved in the chirality degree. Consequently, the branch with positive chirality shows blue-shift, while the negative presents the corresponding red (see also Fig.1(e)). Such a behavior closes the pseudogap at the Fermi energy, thus increasing the amount of the states in the Fermi surface. Therefore, this

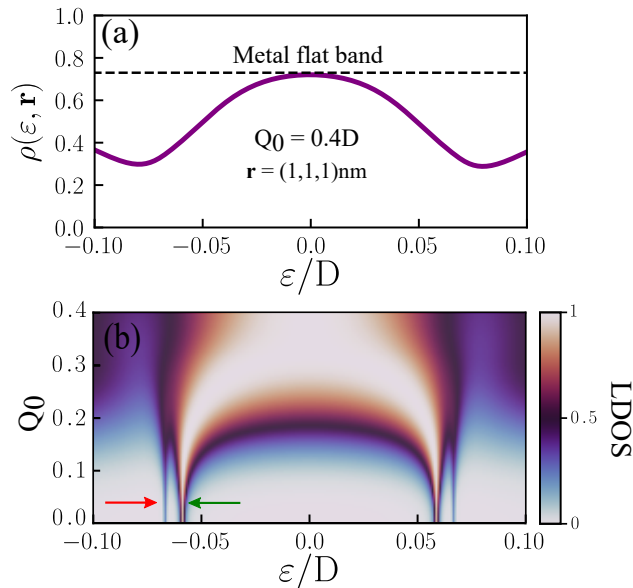


Figure 5. (Color online) Panel (a): The total LDOS of the system consisting of two impurities placed inside a Weyl metal host with $Q_0 = 0.4D$, corresponding to the regime of the formation of an atomic frustrated state. Position of the STM tip is fixed at $\mathbf{r} = (1,1,1)$ nm. Panel (b): Phase diagram, showing the total density of states as function of the energy ε and the parameter Q_0 . With increase of Q_0 one clearly observes the crossover from the regime of standard bonding (indicated by green arrow) and antibonding (indicated by red arrow) molecular orbitals, characterized by four well resolved Hubbard bands, to the regime of frustrated atomic state.

gives rise to the flat metallic-type plateau in the LDOS around $\varepsilon = 0$.

The crossover between the cases of the standard molecular bonding and antibonding states, and formation of an atomic frustrated state is illustrated by Fig. 5(b), where

a phase diagram, showing the total LDOS as function of the energy ε and the parameter Q_0 is presented. With increase of Q_0 the narrow peaks characteristic to four well resolved Hubbard bands become broadened and finally merge, producing characteristic profile plotted in Fig. 5(a). From the experimental perspective, such transition can be achieved by application of stress, which is expected to break the inversion symmetry [13].

IV. CONCLUSIONS

We have demonstrated that the nature of electronic states of a pair of impurities placed inside a Weyl metal strongly depends on the parameter Q_0 , which defines the breaking of the inversion symmetry in the host material. For small values of this parameter one observes the formation of conventional bonding and antibonding molecular orbitals. However, for large values of Q_0 transition to an atomic frustrated state, characterized by a broad bowl-shape distribution of the LDOS in the real space occurs. This transition should take place under the application of external stress, which allows to propose the concept of a molecular switcher, alternating between ordinary molecular and atomic frustrated states.

V. ACKNOWLEDGMENTS

We thank the Brazilian funding agencies CNPq (Grants. 305668/2018-8 and 302498/2017-6), the São Paulo Research Foundation (FAPESP; Grant No. 2018/09413-0) and Coordenação de Aperfeiçoamento de Pessoal de Nível Superior - Brasil (CAPES) – Finance Code 001. YM and IAS acknowledge support the Ministry of Science and Higher Education of Russian Federation, goszadanie no. 2019-1246, and ITMO 5-100 Program.

-
- [1] H. Weyl, *Zeitschrift für Physik* 56, 330 (1929).
 - [2] Z. Wang, Y. Sun, X.-Q. Chen, C. Franchini, G. Xu, H. Weng, X. Dai, and Z. Fang, *Phys. Rev. B* 85, 195320 (2012).
 - [3] Z. K. Liu, B. Zhou, Y. Zhang, Z. J. Wang, H. M. Weng, D. Prabhakaran, S.-K. Mo, Z. X. Shen, Z. Fang, X. Dai *et al.*, *Science* 343, 864 (2014).
 - [4] Z. Wang, H. Weng, Q. Wu, X. Dai, and Z. Fang, *Phys. Rev. B* 88, 125427 (2013).
 - [5] Z. K. Liu, J. Jiang, B. Zhou, Z. J. Wang, Y. Zhang, H. M. Weng, D. Prabhakaran, S.-K. Mo, H. Peng, P. Dudin *et al.*, *Nature Materials* 13, 677 EP– (2014).
 - [6] S.-M. Huang, S.-Y. Xu, I. Belopolski, C.-C. Lee, G. Chang, B. Wang, N. Alidoust, G. Bian, M. Neupane, C. Zhang *et al.*, *Nature Communications* 6, 7373 EP– (2015).
 - [7] H. Weng, C. Fang, Z. Fang, B. A. Bernevig, and X. Dai, *Phys. Rev. X* 5, 011029 (2015).
 - [8] S.-Y. Xu, I. Belopolski, N. Alidoust, M. Neupane, G. Bian, C. Zhang, R. Sankar, G. Chang, Z. Yuan, C.-C. Lee *et al.*, *Science* 349, 613 (2015).
 - [9] B. Q. Lv, H. M. Weng, B. B. Fu, X. P. Wang, H. Miao, J. Ma, P. Richard, X. C. Huang, L. X. Zhao, G. F. Chen *et al.*, *Phys. Rev. X* 5, 031013 (2015).
 - [10] B. Q. Lv, N. Xu, H. M. Weng, J. Z. Ma, P. Richard, X. C. Huang, L. X. Zhao, G. F. Chen, C. E. Matt, F. Bisti *et al.*, *Nature Physics* 11, 724 EP– (2015).
 - [11] S.-Y. Xu, C. Liu, S. K. Kushwaha, R. Sankar, J. W. Krizan, I. Belopolski, M. Neupane, G. Bian, N. Alidoust, T.-R. Chang *et al.*, *Science* 347, 294 (2015).
 - [12] N. Xu, H. M. Weng, B. Q. Lv, C. E. Matt, J. Park, F. Bisti, V. N. Strocov, D. Gawryluk, E. Pomjakushina, K. Conder *et al.*, *Nature Communications* 7, 11006 EP– (2016).
 - [13] N. P. Armitage, E. J. Mele, and A. Vishwanath, *Rev. Mod. Phys.* 90, 015001 (2018).

- [14] X. Wan, A. M. Turner, A. Vishwanath, and S. Y. Savrasov, Phys. Rev. B 83, 205101 (2011).
- [15] K.-Y. Yang, Y.-M. Lu, and Y. Ran, Phys. Rev. B 84, 075129 (2011).
- [16] P. Hosur, S. A. Parameswaran, and A. Vishwanath, Phys. Rev. Lett. 108, 046602 (2012).
- [17] P. Kim, J. H. Ryoo, and C.-H. Park, Phys. Rev. Lett. 119, 266401 (2017).
- [18] H. Nielsen, and M. Ninomiya, Physics Letters B 130, 389–396 (1983).
- [19] G. Xu, , H. Weng, Z. Wang, X. Dai, and Z. Fang, Phys. Rev. Lett. 107, 186806 (2011).
- [20] J.-H. Sun, D.-H. Xu, F.-C. Zhang, and Y. Zhou, Phys. Rev. B 92, 195124 (2015).
- [21] D. Ma, H. Chen, H. Liu, and X. C. Xie, Phys. Rev. B 97, 045148 (2018).
- [22] H.-R. Chang, J. Zhou, S.-X. Wang, W.-Y. Shan, and D. Xiao, Phys. Rev. B 92, 241103 (2015).
- [23] M. V. Hosseini and M. Askari Phys. Rev. B 92, 224435 (2015).
- [24] A. Principi, G. Vignale, and E. Rossi, Phys. Rev. B 92, 041107 (2015).
- [25] S.-H. Zheng, , R.-Q. Wang, M. Zhong, and H.-J. Duan, Scientific Reports 6, 36106 (2016).
- [26] Y. Marques, A. E. Obispo, L. S. Ricco, M. de Souza, I. A. Shelykh, and A. C. Seridonio, Phys. Rev. B 96, 041112 (2017).
- [27] Y. Marques, W. N. Mizobata, R. S. Oliveira, M. de Souza, M. S. Figueira, I. A. Shelykh, and A. C. Seridonio, Scientific Reports 9, 8452 (2019).
- [28] P. W. Anderson, Phys. Rev. 124, 41 (1961).
- [29] J. Hubbard, Proc. R. Soc. A 276, 238 (1963).
- [30] U. Fano, Phys. Rev. 124, 1866 (1961).
- [31] A. E. Miroshnichenko, S. Flach, and Y. S. Kivshar, Rev. Mod. Phys. 82, 2257 (2010).
- [32] H. Bruus and K. Flensberg, Many-Body Quantum Theory in Condensed Matter Physics, An Introduction, Oxford University Press, 2012.
- [33] A. C. Hewson, The Kondo problem to Heavy Fermions, Cambridge University Press, 1993.
- [34] The Hubbard I is applicable for temperatures $T \gg T_K$, being T_K the Kondo temperature. For the evaluation of $\langle n_{j\sigma} \rangle$, T should not be very high so that we can safely assume the Heaviside step function for the Fermi-Dirac distribution $n_F(\varepsilon)$.
- [35] J. Friedel, Il Nuovo Cimento, 7, 287 (1958).